Materials Science & Engineering C 102 (2019) 552–557

Contents lists available at ScienceDirect

Materials Science & Engineering C

journal homepage: www.elsevier.com/locate/msec

Synthesis of multiwall α-Fe_2O_3 hollow fibers via a centrifugal spinning technique

Mandana Akia[a], K. Andre Mkhoyan[b], Karen Lozano[a,*]

[a] Department of Mechanical Engineering, University of Texas Rio Grande Valley, Edinburg, TX 78539, United States of America
[b] Department of Chemical Engineering and Materials Science, University of Minnesota, Minneapolis, MN 55455, United States of America

ARTICLE INFO

Keywords:
α-Fe_2O_3
Centrifugal spinning
Composite
Multiwall
Hollow fibers

ABSTRACT

Hollow hematite (α-Fe_2O_3) fine fibers with multiwall structure were synthesized by utilizing a centrifugal spinning technique. Aqueous solutions of polyvinyl pyrrolidone and iron (III) nitrate nonahydrate were prepared and spun into fibers. The precursor fibers were heat treated at 650 °C to form iron oxide fibers. Scanning electron micrographs revealed the formation of iron oxide hollow fibers with multiwall structure with average wall thickness of 55 ± 15 nm and outer fiber diameter of 852 ± 86 nm. The formation of α-Fe_2O_3 was confirmed by X-ray diffraction analysis and the phase identification was verified by XRD pattern and transmission electron microscopy analysis. These hollow structure α-Fe_2O_3 fibers have promising uses in important biological processes and biomedical applications.

1. Introduction

Methods to synthesize different forms of iron oxide fibers have recently gained interest due to the promising potential applications. Among different structures for iron oxide fibers, hollow fibers structures are of interest for applications in micro-reactors and microfiltration for biological systems [1]. Hematite (α-Fe_2O_3) is the most stable form of iron oxide [2] and its different structures (0-D as nanoparticles and 1-D as nanowires, nanotubes, etc.) are sought for a wide range of applications including in electrochemical energy storage (batteries) [3–7], catalysts [8,9], supercapacitors electrodes [10], water treatment [11–14], biomedical and biological processes [15–20] and gas sensors [21–24]. The sol–gel method for obtaining α-Fe_2O_3 fibers is common techniques to prepare different oxides and composite fibers [25]. For example, Gong et al. [26], reported the application of the sol-gel method for producing hollow α-Fe_2O_3 fibers using ferric alkoxide and acetic acid as starting precursors and alcohol as a solvent. The process of obtaining a sol for developing the fibers, which in their case includes subjecting the system to three heating treatment steps, took more than seven days, and resulted in α-Fe_2O_3 fibers with diameter between 4 and 10 μm and wall thickness of 1–2 μm [26].

The electrospinning technique has been broadly applied to produce solid and hollow nanofibers [7,27–29]. To date, a growing number of studies have reported the fabrication of iron oxide fibers [21,30,31], however few reports have focused on the fabrication of iron oxide hollow fibers. Chaudhari and Srinivasan utilized the electrospinning technique to fabricate α-Fe_2O_3 nanofibers with hollow-structures using $Fe(acac)_3$ and PVP solutions which after fiber formation were subjected to a heat treatment at 450 °C [5]. Zhan et al., fabricated α-Fe_2O_3 hollow fibers using a combined sol–gel and co-electrospinning method followed by calcination at 600 °C for 6 h [32]. Guo et al., synthesized α-Fe_2O_3 hollow nanofibers via electrospinning using $Fe(NO_3)_3$/PVP and dimethylformamide (DMF) as solvent, where the developed composite fibers were calcined at 450 °C [7].

Given the vast number of potential applications of hollow fiber structures, because of their higher surface area, pore size, volume, and lightweight [33], there is a need to develop a cost-effective fabrication process. This study presents an alternative to overcome this challenge. Here we show that the Forcespinning® method, which through the use of centrifugal force, has proven to mass produce fine fibers of a variety of composite, polymeric, and ceramic nanofibers [25,34–36] can be effectively applied to develop hematite hollow fibers.

2. Materials and methods

2.1. Materials and characterization techniques

Polyvinylpyrrolidone (PVP) with average molecular weight of 1,300,000 (99.5%) and ferric nitrate (99% ($Fe(NO_3)_3{\cdot}9H_2O$)) were purchased from Fisher Scientific Co. and used without further

* Corresponding author.
E-mail address: Karen.Lozano@UTRGV.edu (K. Lozano).

https://doi.org/10.1016/j.msec.2019.04.085
Received 10 December 2018; Received in revised form 17 April 2019; Accepted 25 April 2019
Available online 26 April 2019
0928-4931/

modification.

The fibers were produced using a lab scale cyclone from Fiberio Technology Corp. Scanning electron microscopy (SEM) images were obtained using a Sigma VP Carl Zeiss SEM operated at 1 kV. The composite samples were sputtered with gold utilizing a deposition system (Denton's Desk V). The statistical analysis of the fiber diameters was conducted using Image J software and Minitab® 17 software. Thermogravimetric analysis (TGA) and differential thermogravimetric analysis (DTG) were carried out using a SDT Q600 TA TGA in nitrogen flow up to a temperature of 650 °C with a heating rate of 10 °C/min. Conventional transmission electron microscopy (TEM) imaging and scanning transmission electron microscopy (STEM) combined with energy dispersive X-ray spectroscopy (EDX) elemental mapping were conducted on FEI Tecnai G2 F30 and FEI Titan STEMs. The STEM was operated at beam energy of 100 keV. X-ray diffraction (XRD) patterns from the fibers were recorded using a Bruker D8 Advanced X-ray diffractometer in a 2θ range of 10–80° at a scan rate of 1 °C/min. X-ray photoelectron spectroscopy (XPS) analysis was performed using a Thermoscientific Model K-α XPS which utilizes a micro-focused monochromated Al K-α X-ray source with changeable spot size from 30 to 400 μm.

2.2. Fabrication of composite PVP/Iron nitrate and Iron oxide fibers

Composite fibers of PVP/Iron nitrate were fabricated applying a centrifugal spinning method. First a polymer solution of PVP (2.8 g) in 6 g water was prepared and placed under magnetic stirring for at least 3 h. In the meantime, a solution of 1.95 g iron nitrate in 2 g water was prepared. Both solutions were then mixed at room temperature (weight ratio of iron precursor/polymer = 0.7) and stirred for 2 h. The prepared solutions were spun using the cyclone system, the spinneret was fed with 2 ml of solution and fibers spun at a relative humidity between 50 and 60% and an angular velocity of 7000–7500 rpm. The composite fibers were collected as a mat (shinny yellow color). The collected fibers were then subjected to calcination at 650 °C for 2 h with heating rate of 3 °C/min to eliminate the organic compounds and attain iron oxide fibers samples (brown-red color). The fabrication process is shown in Fig. 1.

3. Results and discussions

SEM image in Fig. 2a shows the surface morphology of the developed composite fibers. No particle is seen on the fibers, which indicates a homogenous distribution of the iron nitrate within the sacrificial PVP. The solid structure of the fibers is evident from cross-section also shown in Fig. 2a (upper-right inset). The histogram of diameters of these composite fibers gives an average value of 1243 ± 210 nm (Fig. 2b).

SEM images in Fig. 2c–f show the calcined fibers at different magnifications. Hollow fibers with multiwall structures can be seen. The formation of hollow fibers might be explained by the increase in pressure inside the fibers due to the decomposition of the sacrificial polymer and higher rate of gas evolution (H_2O and CO_2 gases) within the fibers compared to the gas diffusion rate through the fibers resulted in swelling of the fibers to form the hollow structure, which is adjustable based on the heating rate [1,5]. As can be seen from Fig. 2c–f, a uniform hollow multiwall structure is obtained at a heating rate of 3 °C/min at 650 °C. Higher magnification images of these iron oxide fibers depicted the nano-sized multiwall hollow fibers with a coarse surface. Fig. 2e shows a split iron oxide fiber (identified with the red arrow) which exhibits the multiwall continuous hollow canal. The short fibers show hollow structure with an open end which provides a high surface area. Fig. 2f shows that some of iron oxide fibers are double-wall. The analysis indicates that the wall thickness of these fibers are 55 ± 15 nm and a mean outer diameter of 852 ± 86 nm.

TGA and DTG data from pure PVP and PVP/Iron nitrate fibers are shown in Fig. 3a. They represent two steps weight losses at different ranges. The first region of weight loss in the vicinity of 100 °C is attributed to the removal of adsorbed water. The second weight loss peak at 265 °C corresponds to a combined contribution of polymer decomposition and iron precursor. The phase transformation of iron oxide is ascribed to this step, which continues up to the temperature of 400 °C where it becomes stable. In comparison, pure PVP fibers have the degradation temperature above 400 °C (Fig. 1a). Adding the iron salt to the polymer clearly decreased the degradation temperature. The main reason of this behavior was attributed to the interactions of polymer and Fe^{+3} in the spinning process of the developed fibers [1]. For the composite sample, above the temperature of 450 °C, the polymer is burned off and the residual weight of the sample, around 27%, corresponds to the formation of a stable iron oxide phase. The confirmation of the iron oxide phase is provided by X-ray diffraction measurements (Fig. 3b), where presence of peaks 23.8, 33.3, 35.5, 40.9, 49.4, 53.9, 57.5, 62.2, 63.9, 71.9° indicates the formation of α-Fe_2O_3 phase [37].

Fig. 4a shows the XPS spectra for composite PVP/Iron nitrate and iron oxide fibers. As can be seen the peaks correspond to C 1s, O 1s, N 1s, and Fe 2p. For the iron oxide hollow fibers the N 1s peak is negligible which indicates the absence of C—N group. Compared to the composite sample, in iron oxide fibers the relative contents of Fe and O were increased while the carbon content decreased. Fig. 4b, c and d show the deconvolution of Fe 2p, C 1s and O 1s peaks from the composite iron oxide fibers. The peak at binding energy, 710.3 eV is assigned to Fe $2p^{3/2}$ while the peak at 723.1 eV corresponds to Fe $2p^{1/2}$. These peaks are accompanied by satellite peaks corresponding to Fe_2O_3 [37]. As reported in different Fe_2O_3 studies, the presence of the satellite peak between $2p^{3/2}$ and $2p^{1/2}$ with 715.3 eV binding energy (Fig. 4b) confirms the formation of the for α-Fe_2O_3 phase [38] [39]. The deconvolution of C 1s spectrum resulted in two peaks at binding energies

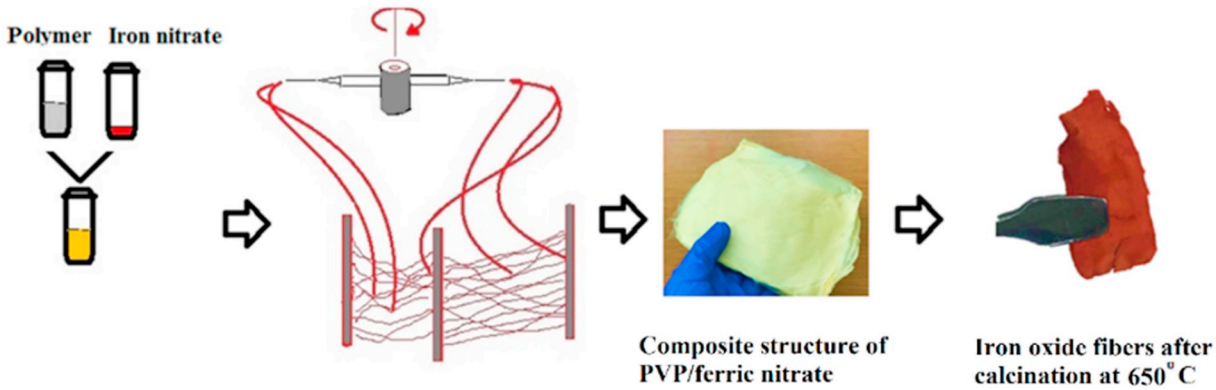

Fig. 1. Schematic representation of fabrication process for α-Fe_2O_3 fibers. Three main steps: solution preparation, spinning, and calcination. (For interpretation of the references to color in this figure, the reader is referred to the web version of this article.)

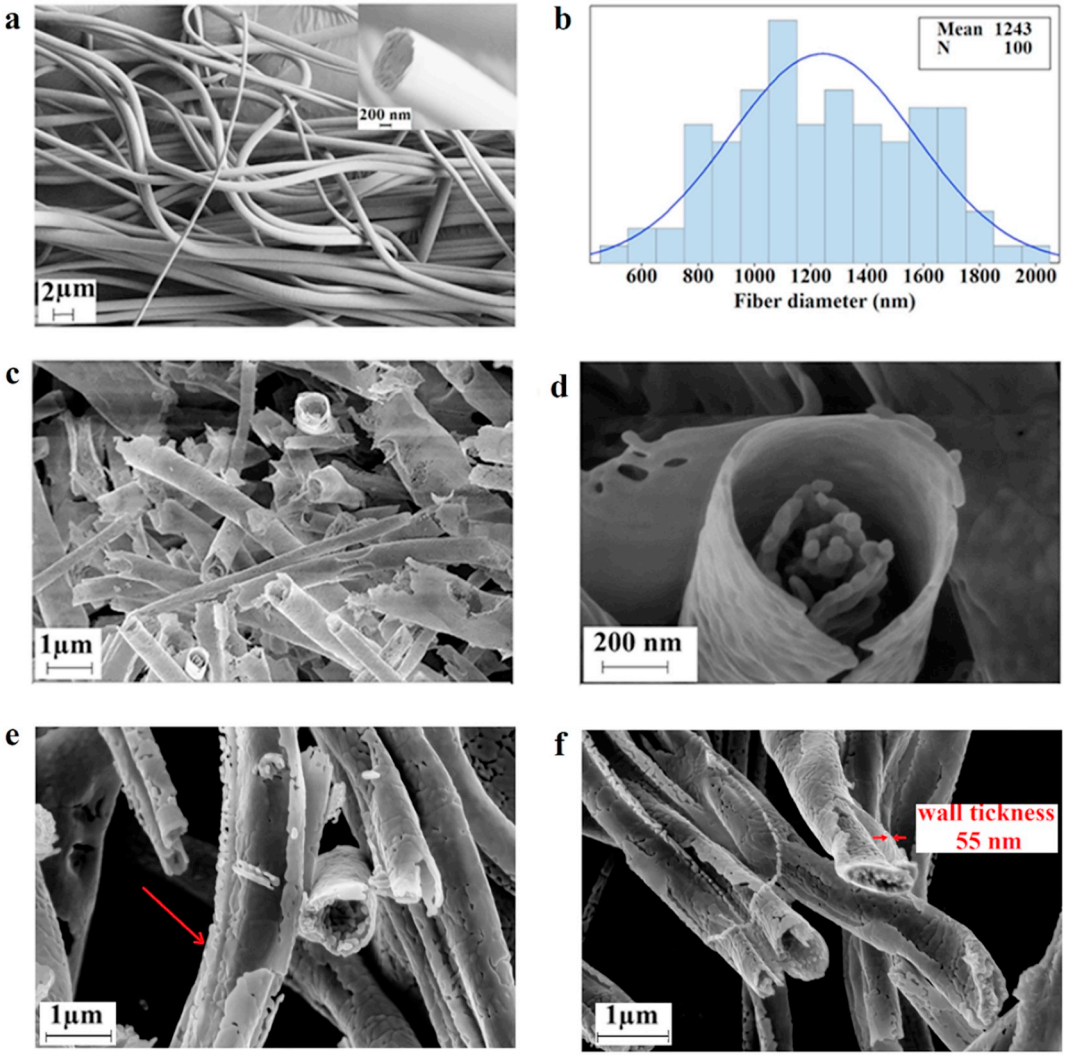

Fig. 2. (a) SEM images of the as prepared PVP/Iron nitrate composite fibers along with its cross section shown in the upper-right inset. (b) The histogram of fiber diameters of these composite fibers. (c, d) SEM images of the fibers calcined at 650 °C obtained at different magnifications. (e, f) Images of split fibers showing uniform hollow structure along the length of the fiber and nano-sized walls of the fabricated iron oxide fibers.

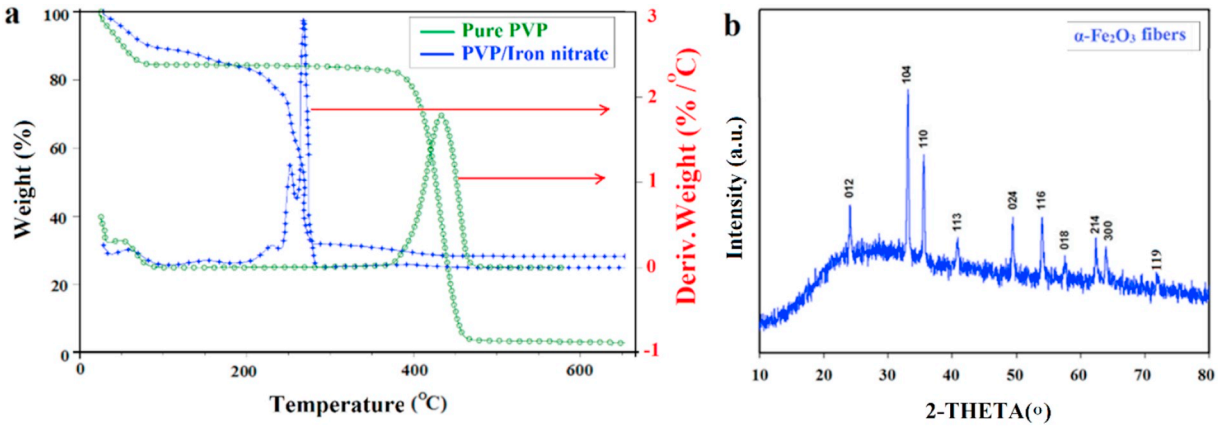

Fig. 3. (a) TGA and DTG data from pure PVP and composite PVP/Iron nitrate fibers and (b) XRD pattern of the fibers calcined at 650 °C.

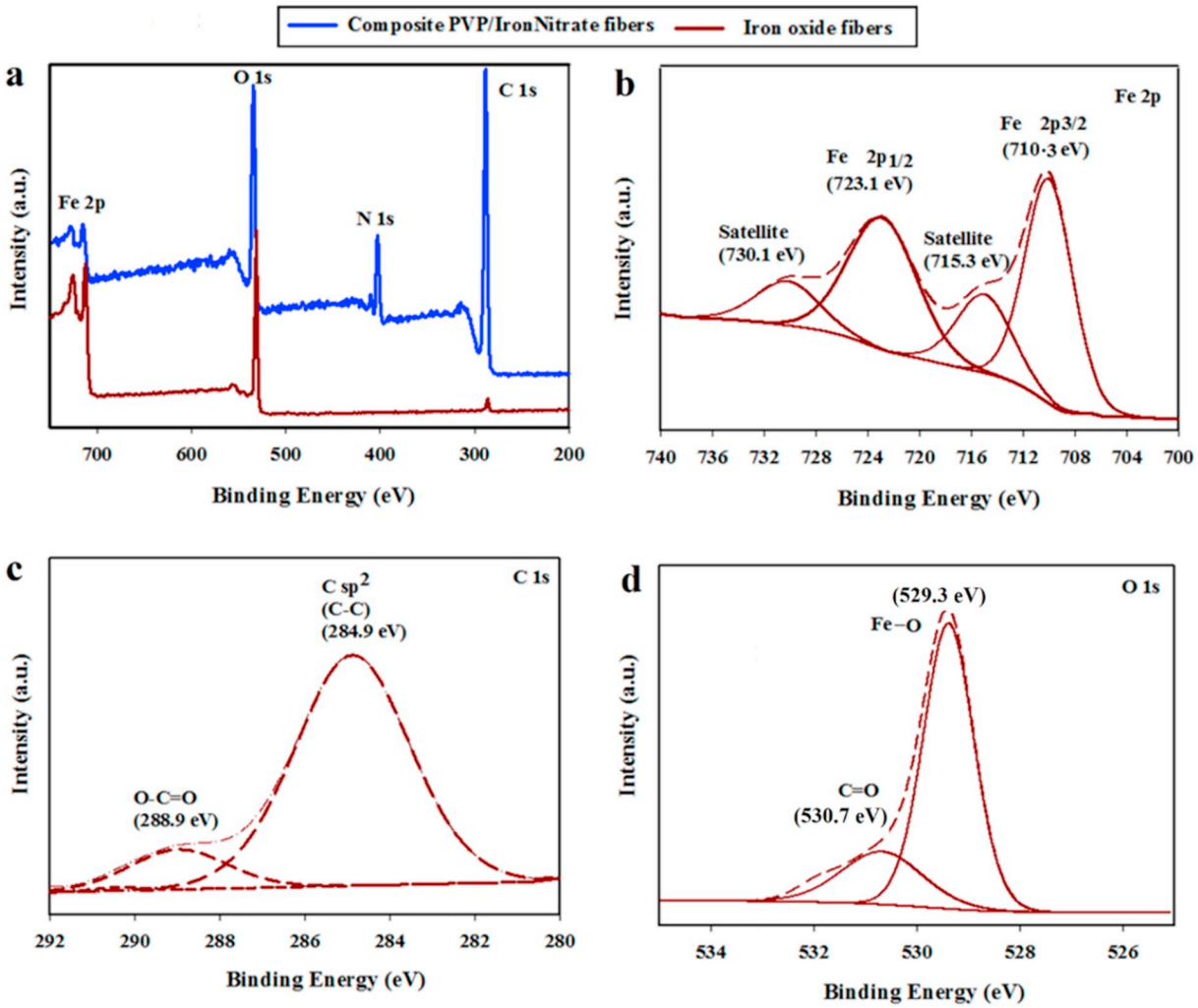

Fig. 4. XPS spectrum for composite and iron oxide fibers samples (a), deconvoluted high resolution XPS spectra of iron oxide fibers for Fe 2p (b), C 1s (c) and O1s (d).

Table 1
Composition of elements in both composite and iron oxide fibers based on the XPS data.

	Carbon (at.%)	Oxygen (at.%)	Iron (at.%)	Nitrogen (at.%)
Composite PVP/Iron nitrate fibers	68.27	20.12	2.52	8.82
Iron oxide fibers	6.27	39.35	53.38	0.28

of 284.9 eV and 288.9 eV attributed to C−C sp^2 and O-C = O bonds respectively. The O 1s peak can also be deconvoluted into two peaks (529.3 and 530.7 eV) and are ascribed to Fe−O, C=O groups [30]. The elemental compositions for the composite sample and iron oxide fibers, based on these XPS data, are reported in Table 1. These results reveal almost 96.5 wt% reduction in the carbon content of the fibers after calcination at 650 °C.

Additional analysis of the crystalline structure and elemental distribution of iron oxide fibers were carried out using analytical STEM (Fig. 5). Fig. 5a shows the high-angle annular dark-field STEM (HAADF-STEM) image and EDX maps of individual Fe, C, and O elementals within the fiber. The EDX maps reveal the presence of Fe and O on the fibers while the EDX elemental analysis at selected points indicates a carbon atomic percentage of 4.5 ± 1.5% within the sample. This result shows the formation of iron oxide fibers and is consistent with XPS elemental composition analysis. HR-TEM image of the fibers (Fig. 5b) shows that fibers are indeed crystalline. The periodic fringes seen in the Fig. 5c matches with (104) plane d-spacing of 0.26 nm in α-Fe_2O_3 lattice. Fast Fourier transform (FFT) obtained from Fig. 5c shows spacings of 2.6 Å and 3.7 Å, which corresponds to d-spacings of (104) and (012) planes respectively (Fig. 5d). These observations agree with the XRD results and further confirm the formation of crystalline α-Fe_2O_3 fibers.

4. Conclusions

Multiwall α-Fe_2O_3 hollow fibers with average wall thickness and fiber diameter of about 55 nm and 850 nm, respectively were fabricated via a simple, flexible, and scalable technique. The precursor fibers with shinny yellow color obtained by centrifugal spinning of an aqueous solution with iron precursor/polymer of 70% w/w were collected as a mat. These initial fibers with diameter of about 1240 nm were PVP/Fe $(NO_3)_3$ fibers. The calcination of the fibers at 650 °C resulted in 32% shrinkage in fibers diameter and a roughening of the surface. The surface morphology of the fabricated multiwall hollow α-Fe_2O_3 fibers with nano-sized wall thickness were studied by SEM. The removal of organic compounds and formation of a stable phase of iron oxide fibers was demonstrated by thermogravimetric analysis. XRD and TEM results confirmed a high purity and crystallinity of the α-Fe_2O_3 hollow fibers. This facile method to fabricate nanolayered multiwall α-Fe_2O_3 hollow fibers renders promising potential for catalysts, biological processes and biomedical applications such as drug delivery carriers.

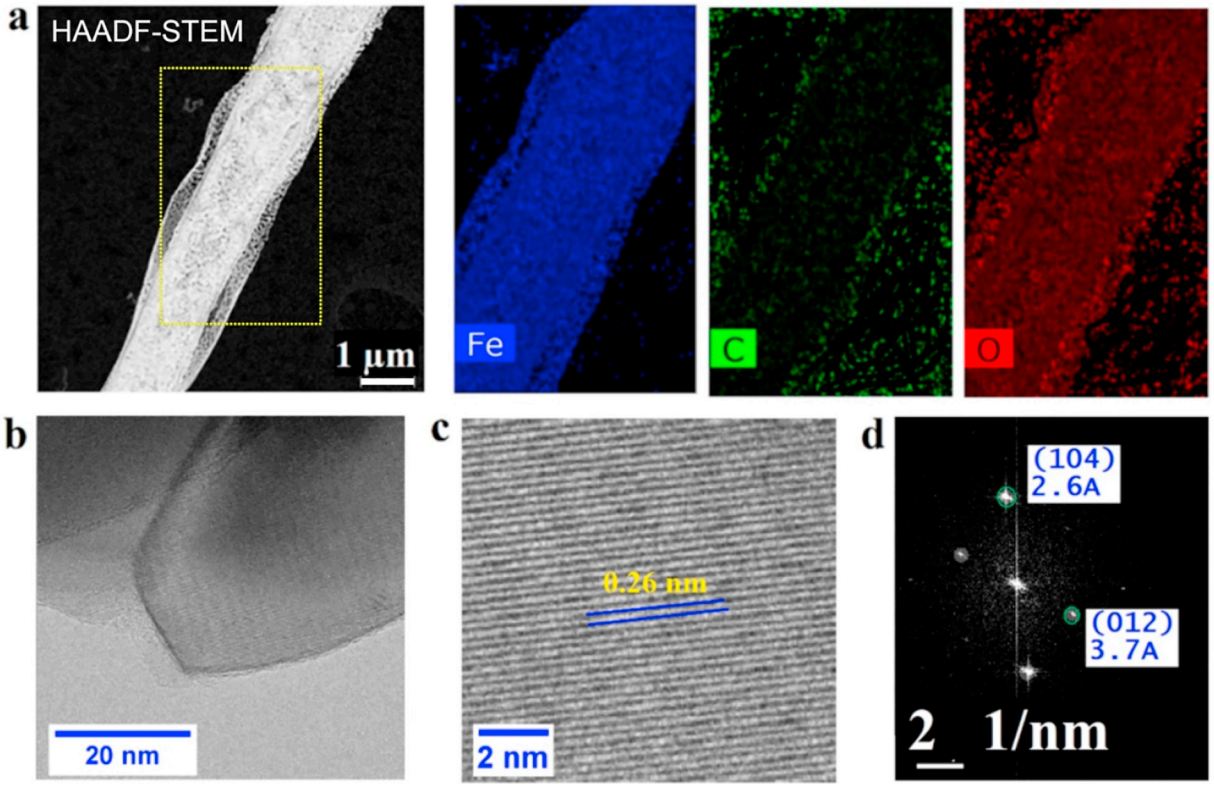

Fig. 5. (a) HAADF-STEM image and a set of EDX elemental maps of an iron oxide fiber obtained from the region indicated in HAADF image by dotted box. (b, c) High-resolution conventional TEM images of the iron oxide fibers showing d-spacing between periodic fringes, and (d) the FFT obtained from the image.

Acknowledgements

This research was supported by NSF PREM award under grant No. DMR-1523577: UTRGV-UMN Partnership for Fostering Innovation by Bridging Excellence in Research and Student Success. This project was partially supported by the MRSEC program of the National Science Foundation under Award DMR-1420013. STEM analysis was performed in the College of Science and Engineering Characterization Facility of the University of Minnesota, which receives partial support from the NSF through the MRSEC program. We also like to thank Dr. Jason Myers and Mr. Jacob Held for their assistance with STEM data acquisition.

References

[1] Y. Cheng, et al., Formation mechanism of Fe2O3 hollow fibers by direct annealing of the electrospun composite fibers and their magnetic, electrochemical properties, CrystEngComm 13 (8) (2011) 2863–2870.
[2] C. Wu, et al., Synthesis of hematite (α-Fe2O3) nanorods: diameter-size and shape effects on their applications in magnetism, lithium ion battery, and gas sensors, J. Phys. Chem. B 110 (36) (2006) 17806–17812.
[3] L. Ji, et al., α-Fe2O3 nanoparticle-loaded carbon nanofibers as stable and high-capacity anodes for rechargeable lithium-ion batteries, ACS Appl. Mater. Interfaces 4 (5) (2012) 2672–2679.
[4] J.S. Cho, Y.J. Hong, Y.C. Kang, Design and synthesis of bubble-nanorod-structured Fe2O3–carbon nanofibers as advanced anode material for Li-ion batteries, ACS Nano 9 (4) (2015) 4026–4035.
[5] S. Chaudhari, M. Srinivasan, 1D hollow α-Fe2O3 electrospun nanofibers as high performance anode material for lithium ion batteries, J. Mater. Chem. 22 (43) (2012) 23049–23056.
[6] J. Ma, et al., FeOx-based materials for electrochemical energy storage, Adv. Sci. 5 (6) (2018) 1–28 (1700986).
[7] J. Guo, et al., Synthesis of α-Fe2O3, Fe3O4 and Fe2N magnetic hollow nanofibers as anode materials for Li-ion batteries, RSC Adv. 6 (112) (2016) 111447–111456.
[8] G. Qiu, et al., Microwave-assisted hydrothermal synthesis of nanosized α-Fe2O3 for catalysts and adsorbents, J. Phys. Chem. C 115 (40) (2011) 19626–19631.
[9] Z. Zhong, et al., Synthesis of porous α-Fe2O3 nanorods and deposition of very small gold particles in the pores for catalytic oxidation of CO, Chem. Mater. 19 (19) (2007) 4776–4782.
[10] G. Binitha, et al., Electrospun α-Fe2O3 nanostructures for supercapacitor applications, J. Mater. Chem. A 1 (38) (2013) 11698–11704.
[11] C.-Y. Cao, et al., Low-cost synthesis of flowerlike α-Fe2O3 nanostructures for heavy metal ion removal: adsorption property and mechanism, Langmuir 28 (9) (2012) 4573–4579.
[12] J. Chang, et al., Preparation of α-Fe2O3/polyacrylonitrile nanofiber mat as an effective lead adsorbent, Environ. Sci.: Nano 3 (4) (2016) 894–901.
[13] Y. Liu, et al., Fast degradation of methylene blue with electrospun hierarchical α-Fe2O3 nanostructured fibers, J. Sol-Gel Sci. Technol. 58 (3) (2011) 716.
[14] Q. Gao, et al., Novel hollow α-Fe2O3 nanofibers via electrospinning for dye adsorption, Nanoscale Res. Lett. 10 (1) (2015) 176.
[15] T.-S. Kim, et al., Carbon-decorated iron oxide hollow granules formed using a silk fibrous template: lithium-oxygen battery and wastewater treatment applications, NPG Asia Mater. 9 (2017) e450.
[16] H.-M. Fan, et al., Single-crystalline MFe2O4 nanotubes/nanorings synthesized by thermal transformation process for biological applications, ACS Nano 3 (9) (2009) 2798–2808.
[17] S.J. Son, et al., Magnetic nanotubes for magnetic-field-assisted bioseparation, biointeraction, and drug delivery, J. Am. Chem. Soc. 127 (20) (2005) 7316–7317.
[18] S. Ramaswamy, et al., Magnetic resonance imaging of chondrocytes labeled with superparamagnetic iron oxide nanoparticles in tissue-engineered cartilage, Tissue Eng. A 15 (12) (2009) 3899–3910.
[19] D. Nieciecka, et al., Solid-core and hollow magnetic nanostructures: synthesis, surface modifications and biological applications, Bioelectrochemistry 93 (2013) 2–14.
[20] K. An, T. Hyeon, Synthesis and biomedical applications of hollow nanostructures, Nano Today 4 (4) (2009) 359–373.
[21] W. Zheng, et al., Electrospinning route for α-Fe2O3 ceramic nanofibers and their gas sensing properties, Mater. Res. Bull. 44 (6) (2009) 1432–1436.
[22] L. Wang, et al., Three-dimensional hierarchical flowerlike α-Fe2O3 nanostructures: synthesis and ethanol-sensing properties, ACS Appl. Mater. Interfaces 3 (12) (2011) 4689–4694.
[23] L. Wang, et al., Ethanol gas detection using a yolk-shell (core-shell) α-Fe2O3 nanospheres as sensing material, ACS Appl. Mater. Interfaces 7 (23) (2015) 13098–13104.
[24] Y. Huang, et al., A high performance hydrogen sulfide gas sensor based on porous α-Fe2O3 operates at room-temperature, Appl. Surf. Sci. 351 (2015) 1025–1033.
[25] M. Akia, et al., Development and optimization of alumina fine fibers utilizing a centrifugal spinning process, Microporous Mesoporous Mater. 262 (2018) 175–181.
[26] C. Gong, et al., Continuous hollow α-Fe2O3 and α-Fe fibers prepared by the sol–gel method, J. Mater. Chem. 12 (6) (2002) 1844–1847.
[27] D. Li, Y. Xia, Direct fabrication of composite and ceramic hollow nanofibers by electrospinning, Nano Lett. 4 (5) (2004) 933–938.
[28] A. Greiner, J.H. Wendorff, Electrospinning: a fascinating method for the

preparation of ultrathin fibers, Angew. Chem. Int. Ed. 46 (30) (2007) 5670–5703.
[29] J.T. McCann, D. Li, Y. Xia, Electrospinning of nanofibers with core-sheath, hollow, or porous structures, J. Mater. Chem. 15 (7) (2005) 735–738.
[30] X. Chen, et al., Fabrication, formation mechanism, and magnetic properties of metal oxide nanotubes via electrospinning and thermal treatment, J. Phys. Chem. C 115 (2) (2010) 373–378.
[31] Y. Zhu, et al., Preparation of superhydrophilic α-Fe2O3 nanofibers with tunable magnetic properties, Thin Solid Films 510 (1–2) (2006) 271–274.
[32] S. Zhan, et al., Facile fabrication of long α-Fe2O3, α-Fe and γ-Fe2O3 hollow fibers using sol–gel combined co-electrospinning technology, J. Colloid Interface Sci. 308 (1) (2007) 265–270.
[33] J. Huang, et al., Selective fabrication of porous iron oxides hollow spheres and nanofibers by electrospinning for photocatalytic water purification, Solid State Sci. 82 (2018) 24–28.
[34] M. Akia, et al., High-throughput production with improved functionality and graphitization of carbon fine fibers developed from sodium chloride-poly-acrylonitrile precursors, Polym. Eng. Sci. 58 (11) (2018) 2047–2054.
[35] M. Akia, et al., In situ production of graphene–fiber hybrid structures, ACS Appl. Mater. Interfaces 9 (30) (2017) 25474–25480.
[36] K. Sarkar, et al., Electrospinning to forcespinning™, Mater. Today 13 (11) (2010) 12–14.
[37] X. Hu, et al., α-Fe2O3 nanorings prepared by a microwave-assisted hydrothermal process and their sensing properties, Adv. Mater. 19 (17) (2007) 2324–2329.
[38] E. Samuel, et al., Carbon nanofibers decorated with FeOx nanoparticles as a flexible electrode material for symmetric supercapacitors, Chem. Eng. J. 328 (2017) 776–784.
[39] B. Patil, et al., Electrochemical performance of a coaxial fiber-shaped asymmetric supercapacitor based on nanostructured MnO2/CNT-web paper and Fe2O3/carbon fiber electrodes, Carbon 134 (2018) 366–375.